Nanoscale

Accepted Manuscript

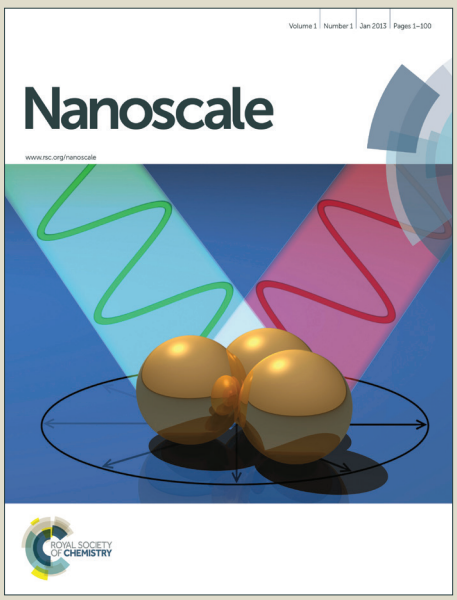

ROYAL SOCIETY OF CHEMISTRY

www.rsc.org/nanoscale

Cite this: DOI: 10.1039/c0xx00000x

www.rsc.org/xxxxxx

ARTICLE TYPE

Bottom-up preparation of MgH_2 nanoparticles with enhanced cycle life stability during electrochemical conversion in Li-ion batteries

Yassine Oumellal[a], Claudia Zlotea[*a], Stéphane Bastide[a], Christine Cachet-Vivier[a], Eric Léonel[a], Stéphane Sengmany[a], Eric Leroy[a], Luc Aymard[b], Jean-Pierre Bonnet[b], Michel Latroche[a]

Received (in XXX, XXX) Xth XXXXXXXXX 20XX, Accepted Xth XXXXXXXXX 20XX
DOI: 10.1039/b000000x

A promising anode material for Li-ion batteries based on MgH_2 with around 5 nm average particles size was synthesized by a bottom-up method. A series of several composites containing well dispersed MgH_2 nanoparticles into a porous carbon host has been prepared with different metal content up to 70 wt.%. A narrow particle size distribution (1-10 nm) of the MgH_2 nanospecies with around 5.5 nm average size can be controlled up to 50 wt.% Mg. After a ball milling treatment under Ar, the composite containing 50 wt.% Mg shows an impressive cycle life stability with good electrochemical capacity around 500 $mAh.g^{-1}$. Moreover, the nanoparticles size distribution is stable during cycling.

Introduction

Nanomaterials and nanostructures play an important role in the recent development of modern technologies that requires the use of versatile and multifunctional materials.[1] Beside a wide range of possible applications, nanomaterials have already proven unique advantages and enhanced specific properties in the field of clean energy applications, essentially energy storage and conversion.[2,3] The energy related applications concern the use of nanostructured materials in different fields such as, photovoltaic, electrodes in Li-ion batteries, supercapacitors and hydrogen storage. Each particular application has different material related challenges that need to be overcome for future large scale utilization in practical devices.

The energy conversion and storage involve physical interactions and/or chemical reactions at the surface or interface as well as diffusion of different species within the materials. The use of nanomaterials holds promise to improve their specific properties due to both increased surface/interface area, which is important for rapid charge transfer, and short length scales within the materials, that are essential for fast charge and mass transport phenomena. Two synthetic methods are used to prepare nanomaterials: either top-down or bottom-up strategies in harsh or mild conditions, respectively. The main drawback of such nanomaterials is the particle tendency to grow into large aggregates with minimum surface energy and bulk-like behaviour. Therefore, the stabilization of active species at nanoscale is essential to hinder their coalescence and to retain their nanosized dimension upon cycling.

The encapsulation or confinement strategies in the design of energy storage and conversion materials is an emerging synthetic route that shows promising results.[4,5] Indeed, for solid-state hydrogen storage applications, very fast hydrogen absorption/desorption kinetics have been confirmed for nanoscaled Mg hydride (MgH_2) confined into the porosity of different carbon hosts.[6,7] Moreover, the increased contribution of surface energy may change the thermodynamic of reaction with hydrogen, as proven for nanosized MgH_2 confined into different matrices.[8,9] These nanoconfined hydrides for hydrogen storage purposes have been prepared by both top-down and bottom-up methods.

For energy conversion applications, the use of nanostructured materials as electrode for Li-ion batteries has been widely studied during the last decade; the most attractive materials are silicon and oxides.[10–14] These nanostructured materials offer advantages such as, large specific area for fast faradic reaction, small distances for faster lithium mass diffusion and charge transport. Recently, metal hydrides have been shown to be very promising electrodes in Li-ion batteries thanks to their high gravimetric and volumetric capacities, low polarization and a suitable equilibrium potential for application as anode material.[15–19] Metal hydrides are able to electrochemically react with lithium according to the conversion reaction $MH_x + x\mathrm{Li}^+ + x\mathrm{e}^- \leftrightarrows M + x\mathrm{LiH}$. The reversibility of this reaction at reasonable regime requires the use of nano-hydrides to favour charge transfer at the MH/electrolyte interface on lithiation and mass transfer between M and LiH phases during delithiation. Furthermore, nanosizing prevents losing of electronic percolation within the electrode due to volume changes on lithiation/delithiation and, therefore, leads to enhanced electrode cycle-life. Among hydrides, MgH_2 is very attractive because of its high theoretical gravimetric (2038 $mAh.g^{-1}$) and volumetric capacities as well as safe potential window of 0.1–0.5 V versus Li^+/Li^0. So far, MgH_2, as electrode nanomaterial in Li-ion batteries, has been synthesized by the top-down ball milling method starting from bulk state.[15,20,21]

The present report describes the fundamental and electrochemical

conversion properties of composite materials containing MgH_2 nanoparticles synthesized by a bottom-up chemical method. Well dispersed MgH_2 nanoparticles with an average size around 5 nm are stabilized into a porous carbon host. A series of several composites has been prepared with different metal loadings ranging from 15 to 70 wt.% Mg. To our knowledge, this is the first time that Mg-based composites prepared by bottom-up method with high Mg loadings are reported for electrochemical conversion in Li-ion batteries. A thorough electrochemical investigation was carried out for the composite with 50 wt.% Mg, *i.e.* containing the maximum of MgH_2 active nanospecies with well controlled particle size distribution.

Experimental details

Synthesis of nanosized MgH_2

A series of composites has been synthesized by bottom-up wet impregnation method with different Mg loadings. In-depth report of the bottom-up synthesis can be found elsewhere.[6] The commercial High Surface Area Graphite (TIMREX®HSAG-500) has been chosen as porous scaffold due to its high chemical purity and inertness towards MgH_2. It possesses a relatively high surface area (500 $m^2.g^{-1}$) and contains mesopores mostly around 3-4 nm and up to 20 nm.

A commercial molar solution of $MgBu_2$ (Sigma Aldrich) was used for the liquid impregnation of the porous carbon host. After solvent removal by heating at moderate temperature (353 K) into an Ar flow, the hydrogenation of the Mg precursor was performed under hydrogen at 5 MPa and 423 K. This reaction produces well distributed MgH_2 nanoparticles directly into the carbon host and releases C_4H_{10} gas, as already shown in previous studies.[7,6,22,23] The nominal chemical compositions of the composites are 15, 25, 50 and 70 wt.% Mg relative to the final mass. The MgH_2 concentrations and consequently, the hydrogen content in the composites, were fixed by the amount of $MgBu_2$ precursor used for carbon impregnation. The composites will be further named *x*MgH_2@HSAG-500, where *x* stands for 15, 25, 50 and 70. All composites are extremely reactive to air or moisture and consequently stored and manipulated inside a purified Ar glove box.

X-ray powder diffraction

The structural properties of composites have been characterized by X-ray powder diffraction (XRD) using a D8 advanced Bruker diffractometer (Cu K_α radiation). Due to the high reactivity of composites to air moisture, all XRD measurements have been performed under Ar atmosphere with the help of a specially designed air-tight sample holder.

Microstructural measurements

Microstructural observations were performed by Transmission Electron Microscopy (TEM) with a 200 kV FEG TEM (FEI Tecnai F20, point resolution 0.24 nm). The composites have been transferred in the microscope by the help of an air-tight sample holder. The sample holder was cooled down to 110 K to avoid sample decomposition by beam irradiation. Due to weak chemical contrast between metal nanoparticles and carbon host, dark field TEM images have been mainly recorded. A typical dark field TEM image together with the corresponding SAED pattern of one composite is shown in the SI (figure SI-1). All diffractions spots can be indexed in the tetragonal MgH_2 structure (JCP: 01-74-0934) confirming that neither decomposition nor oxidation occurs during this measurement. The MgH_2 particle size distribution and mean size (if applicable) have been determined by statistical analyses of several TEM images (Table 1). After electrochemical cycling the composites have been characterized by TEM. The powder was collected from the cycled electrode inside the glove box and rinsed with dimethyl carbonate to remove possible $LiPF_6$ traces.

Textural properties

The textural properties have been determined by nitrogen adsorption isotherm at 77 K using an Autosorb IQ Quantachrome instrument (Figures SI-2 and SI-3). The samples have been loaded inside an Ar glove box and transferred to the instrument under protective atmosphere. Prior to measurements, the samples have been degassed under secondary vacuum at 473 K for 12 hours. The specific surface area was obtained by the Brunauer-Emmett-Teller (BET) method within the 0.05-0.25 relative pressure range, the microporous volume was determined by the Dubinin-Radushkevich (DR) equation below 0.05 relative pressure the and the total porous volume was calculated at a relative pressure P/P_0 of 0.97.[24] The textural properties are given per gram of composite (Table 1).

Ball-milling treatment

A Fritsch Pulverisette 7 mixer located inside an Ar glove box was used to mill the as-synthesized composite at 800 rpm for 10 hours in a 25 ml stainless-steel milling container with a ball to powder weight ratio of 10.

Electrochemical characterizations

Electrochemical measurements (see Figures SI-4, SI-5 and SI-6) were performed in Swagelok and/or coin half cells, assembled in an Ar glove box and cycled using a VMP automatic cycling/data recording system (Biologic Co.). A ~10 mg positive electrode was prepared by mixing 80 wt.% of *x*MgH_2@HSAG-500 composite with 20 wt.% of conducting agent (SP carbon from Sigma Aldrich). The negative electrode was made of a 1 cm^2 Li metal disc. The positive and negative electrodes were separated by a Whatman GF/D borosilicate glass-fibre sheet saturated with a 1M $LiPF_6$ electrolyte solution in 1:1 dimethyl carbonate/ethylene carbonate as the electrolyte. The assembled cells were galvanostatically cycled with a voltage window between 3 and 0.005 V (vs. Li^+/Li^0) at a constant C-rate of 1 lithium in 10 hours. The electrochemical capacity is calculated over the weight of the MgH_2 content and the carbon contribution was neglected. Additional measurements given in ESI allow supporting this hypothesis (Figure SI-5).

Results and discussions

As-synthesized composites

xMgH_2@HSAG-500 composites have been synthesized with different metal loadings, *x* = 15, 25, 50 and 70 wt.%. All as-synthesized composites are biphasic containing the pristine carbon HSAG-500 (hexagonal $P6_3/mmc$) and the MgH_2 nanoparticles (tetragonal $P4_2/mnm$), as noticed in the XRD

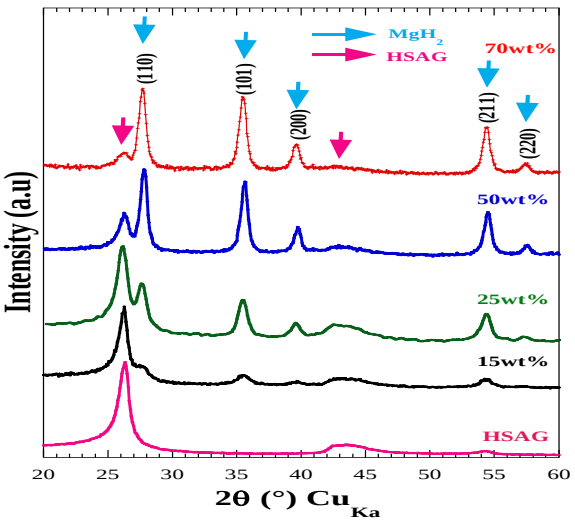

Fig.1 X-ray diffraction patterns of xMgH$_2$@HSAG with x = 0, 15, 25, 50 and 70 wt.% Mg.

patterns (Figure 1). The graphitic carbon host is structurally unchanged during the synthesis of MgH_2 nanoparticles, in agreement with our previous study.[6] The intensity of the diffraction peaks of the MgH_2 phase is gradually rising together with slight peak narrowing with increasing metal content. This suggests that the MgH_2 crystallite size steadily increases with metal loading. The use of the Scherrer formula to determine the MgH_2 crystallite size was not presently applied since it has been already shown to give inappropriate results on this type of composite.[6]

Previously, composites with Mg content up to 20-25 wt.% have been reported for solid-state hydrogen storage.[6,7,23,25] For these concentrations, all Mg-based nanoparticles are believed to be stabilized/confined into the pores and consequently, their size is limited by the pore size distribution of the carbon scaffolds.

One earlier publication describes the effect of high Mg loading (up to 90 wt.%) in mesoporous carbon on the kinetics and thermodynamics of hydrogen absorption/desorption.[22] It is believed that high Mg loadings favour the formation of Mg-based nanoparticles outside the available pores on the external surfaces of the carbon hosts. This may result in particle agglomeration and loss of control of particle size distribution during hydrogen absorption/desorption cycling, which makes the interpretation of experimental results questionable.[26] It is therefore, important to clearly determine the maximum Mg concentration that offers narrow and controlled MgH_2 particle size distribution for electrochemical conversion purposes. Moreover, the majority of nanoparticles should be stabilized into the pores of the carbon host in order to limit possible coalescence during electrochemical cycling since agglomeration of such small MgH_2 nanoparticles has been already observed during hydrogen absorption/desorption cycling at 573 K.[26]

The direct proof of the evolution of MgH_2 nanoparticles size distribution with metal loading is brought by TEM investigations. Dark field TEM images for all as-synthesized composites are depicted in Figure 2 together with their corresponding MgH_2 nanoparticle size distribution histograms. MgH_2 nanoparticles are noticed as bright spots in the dark field TEM images and are well dispersed into the porous carbon host, irrespective of the Mg loading. The particle size distributions are very narrow for low Mg concentration (15 and 25 wt.%) and gradually expands for high metal loading (50 and 70 wt.%). This trend is in good agreement with XRD results. For low loadings (15 and 25 wt.%), the Mg content does not affect the particle size distribution and average particle sizes. The majority of the MgH_2 nanoparticles have sizes below 10 nm with an average particle size around 4-5 nm (Table 1), which is comparable to the mean pore size of the carbon scaffold (3-4 nm). Very few large nanoparticles between 10-20 nm can be noticed for these two composites. The narrow particle size distributions and the good agreement between average particle sizes and available carbon pore sizes suggest that MgH_2 nanoparticles are well confined into pores of carbon host for low Mg contents (15 and 25 wt.%).

For higher Mg loading, particle size distributions show large asymmetric tails up to 35 and 60 nm for 50 and 70 wt.% Mg, respectively. Most of the nanoparticles are below 10 nm size with an average particle size of 5.5 nm in the case of 50MgH$_2$@HSAG-500 (Table 1). For the highest Mg loading (70 wt.%), proposing an average particle size is meaningless due to the broad particle size distribution (up to 60 nm). As suggested above, the MgH_2 nanoparticles with sizes below 4 nm are possibly confined into the pores of carbon. Although larger porosity (up to 20 nm) is available in the carbon scaffold, the MgH_2 nanoparticles with sizes above 20 nm are probably laying on the external surface of the composites.

As a conclusion from the TEM measurements, Mg loading controls the particle size distribution and the average size of MgH_2 particles. For Mg content up to 50 wt.%, the particle size distribution is narrow and most of the nanoparticles are below 10 nm with an average particle size between 4 and 5.5 nm. However, a clear conclusion about the effective nanoconfinement cannot be drawn from solely particle size distribution.

To check the successful confinement of MgH_2 nanoparticles into the pores, the textural properties of all composites have been determined by N_2 sorption isotherms recorded at 77 K (Table 1 and Figures SI-2 and 3 in SI).

Table 1. Textural properties and the average size of MgH_2 nanoparticles, as determined by TEM, for all as-synthesized xMgH$_2$@HSAG-500 composites and ball milled 50MgH$_2$@HSAG-500. For the highest Mg loading, the particle size distribution is too large for proposing an average MgH_2 size.

Composite	Mg content (wt.%)	S_{BET} ($m^2.g^{-1}$) (±20)	V_{tot} ($cm^3.g^{-1}$) (±0.02)	V_{DR} ($cm^3.g^{-1}$) (±0.01)	<MgH_2> size (nm) (±1)
HSAG-500	0	500	0.68	0.02	-
15MgH$_2$@ HSAG-500	15	255	0.37	0.07	4.0
25MgH$_2$@ HSAG-500	25	264	0.37	0.08	5.0
50MgH$_2$@ HSAG-500	50	211	0.30	0.06	5.5
BM 50MgH$_2$@ HSAG-500	50	75	0.10	-	5.0
70MgH$_2$@ HSAG-500	70	201	0.31	0.05	-

Cite this: DOI: 10.1039/c0xx00000x

www.rsc.org/xxxxxx

ARTICLE TYPE

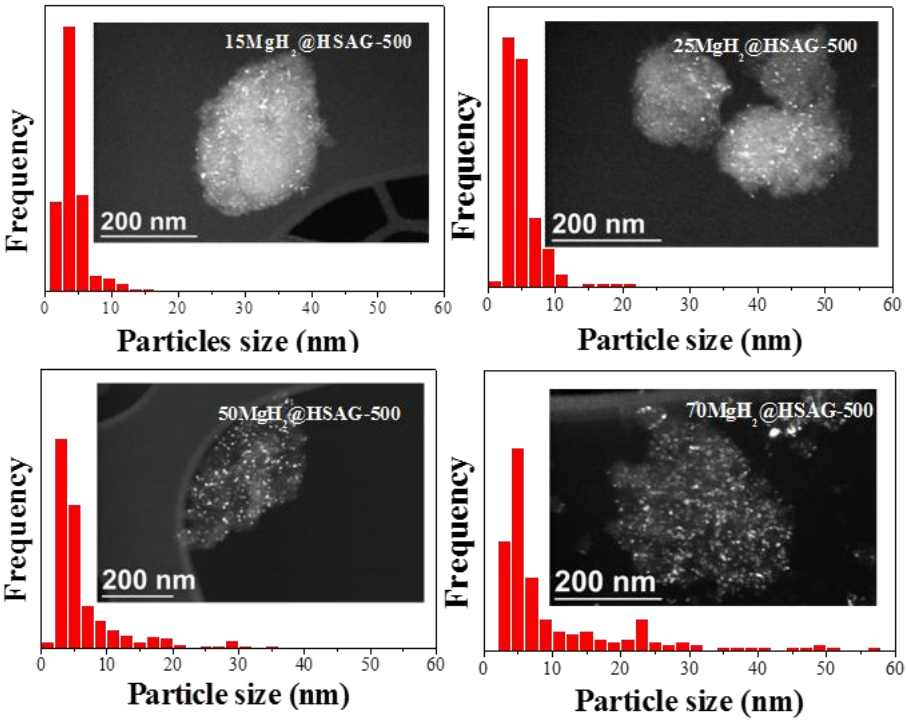

Fig.2 Dark field TEM images and corresponding MgH_2 nanoparticle size distribution histograms for the *x*MgH_2@HSAG-500 composites (*x* = 15, 25, 50 and 70 wt.% Mg).

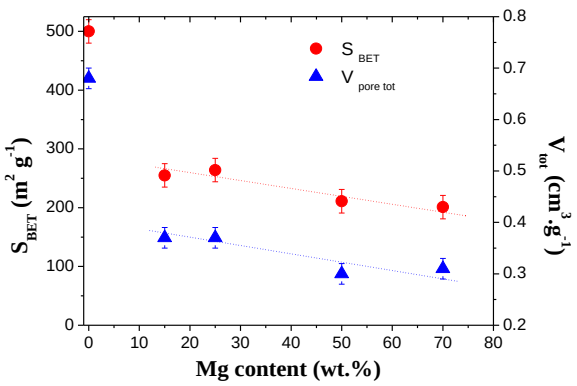

Fig.3 Specific surface area (S_{BET}) and total porous volume (V_{tot}) of *x*MgH_2@HSAG-500 composites versus Mg loading in wt.%. The dotted lines are guide for the eyes.

Figure 3 displays the evolution of the textural properties (specific surface area S_{BET} and total porous volume V_{tot}) as function of Mg content. The insertion of metal nanoparticles into porous scaffolds decreases both specific surface area S_{BET} and total porous volume V_{tot} and both values are evolving similarly with Mg content. This can be explained by the increase of the total weight of the final composites as well as a blocking of available pores by nanoparticles.[4,27]

Strong reductions of S_{BET} and V_{tot} arise for low Mg content and the textural properties are regularly decreasing for further metal loadings. This confirms that MgH_2 nanoparticles are effectively confined in the carbon porosity for low Mg concentrations, as also suggested from TEM nanoparticles size distributions.

The volume of MgH_2 nanoparticles estimated from the bulk density (1.45 $cm^3.g^{-1}$) and the metal concentration can be compared to the available porous volume of the carbon scaffold. For the 50 wt.% Mg concentration, the MgH_2 volume (~ 0.34 $cm^3.g^{-1}$) matches the available porous volume of carbon scaffold (~ 0.34 $cm^3.g^{-1}$, corresponding to half of pore volume of the pristine carbon). Tentatively, if the entire pore volume of carbon is fully occupied by MgH_2 nanoparticles, the overall porosity of the 50MgH_2@HSAG-500 composite would be close to zero. However, small porosity is still observed for this composite, which suggests that the nanoconfinement of MgH_2 is partial. MgH_2 nanoparticles are both confined into the nanopores and supported on the external surface of the carbon host, although their exact ratio is difficult to assess.

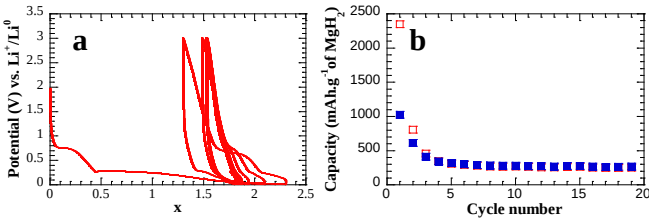

Fig.4 Potential/composition profile for the first 5 cycles of as-synthesized 50MgH_2@HSAG-500 (a) and discharge (red) and charge (blue) capacities during 20 cycles (b).

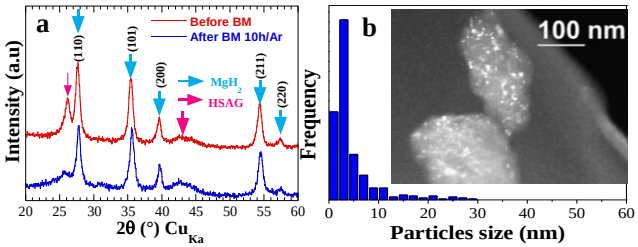

Fig.5 X-ray diffraction patterns of 50MgH_2@HSAG-500 before and after 10 h of ball-milling (a) and nanoparticles histogram and TEM dark field image after ball milling (b).

Tuning the Mg loading in *x*MgH_2@HSAG-500 composites leads to controlled MgH_2 nanoparticles size up to a maximum concentration of 50 wt.%. From the analysis of both TEM particle size distributions and textural properties it can be concluded that MgH_2 particles are mainly nanoconfined into the pores, though some of them can be supported on the external surfaces of the carbon scaffold. For the purpose of electrochemical conversion in Li-ion batteries, the exact ratio of nanoparticles within and outside the pores is less significant than the control of their size and does not jeopardize further interpretation of the experimental results. Higher Mg content expands the particle size distribution up to 60 nm and consequently the amount of nanoparticles supported on the external surfaces.

All as-synthesized *x*MgH_2@HSAG-500 composites as well as the pristine HSAG-500 have been tested as negative electrodes for the conversion reaction with Li (Figure SI-4 and SI-6). Figure 4 depicts the potential/composition profile and the capacity versus cycle number of the as-synthesized 50MgH_2@HSAG-500. This latter composite has been chosen for a systematic electrochemical investigation since it contains the maximum amount of MgH_2 active nanospecies with well controlled particle size distribution. The reversible electrochemical capacity strongly drops after few cycles suggesting a rapid loss of electronic contact between active MgH_2 particles and the carbon host.

It is worth noting that this result is obtained without ball milling pre-treatment or electrode formulation. Yet the electrochemical performance is comparable to the ball milled MgH_2 material with Cu foam as conductive matrix within the same potential window.[15]

Ball-milled 50MgH_2@HSAG-500 composite

Ball-milling is known to optimize material microstructures and is widely used in the field of catalysis, hydrogen storage or lithium ions batteries. In the present work the ball-milling is anticipated to improve the electrical contacts between the grains as well as between the MgH_2 nanoparticles and the carbon host, which are very important to achieve good reversible capacity and cycle life stability. Such treatment could reduce the total cell polarization and facilitate the conversion reaction kinetics, leading to an improvement of the electrochemical properties.

The structural, textural and microstructural properties of ball-milled composite (BM50MgH_2@HSAG-500) have been determined and are compared to the as-synthesized material. The XRD patterns and TEM measurements are shown in Figure 5. The ball-milling treatment leads to the amorphization of the HSAG-500 graphite (Figure 5a). The values of the Full Width at Half Maximum (FWHM) of the strongest MgH_2 diffraction peaks are comparable before and after ball-milling. This indicates that this treatment does not affect the crystallinity and crystal size of MgH_2. Moreover, the MgH_2 particle size distribution is unchanged with an average particle size around 5 nm (Figure 5b). Textural properties strongly decrease after ball milling (Figure SI-3 and Table 1).

Electrochemical performances of ball milled 50MgH_2@HSAG-500

The potential composition profiles and the corresponding differential curves of BM50MgH_2@HSAG-500 composite are plotted in Figure 6. The global electrochemical behaviour is in good agreement with that of MgH_2 previously reported in the literature.[15,20,21] In all previous works, ball-milled MgH_2 was prepared by top-down method from bulk (commercial or synthesized by solid-gas reaction). The electrochemical behavior showed well defined plateaus (conversion + alloying reactions) in the potential composition curves, which facilitates the discrimination between these two reactions. In the present work, the ball-milled nanometric MgH_2 prepared by bottom-up method shows poorly defined plateaus at lower voltages, which makes the discrimination of the reactions less obvious than in the previous case. To help a clear distinction between these reactions, a thorough discussion will be given on the basis of differential curves of potential composition profiles.

Firstly, the differential curve (Figure 6b) during the first discharge (Figure 6a) clearly shows the presence of three cathodic peaks: the first one at 0.75 V is due to the reaction of the carbon with lithium to form the Solid Electrolyte Interface (SEI); a second intense peak at 0.21V is attributed to the conversion reaction of MgH_2 with lithium and corresponds to the well-defined plateau recorded on the potential/composition profile; the third one located at 0.08 V is assigned to the alloying reaction of magnesium (Mg^0) with lithium ions. For further cycles (Figure 6c and d), the conversion reaction peak jumps from 0.21 to 0.31 V and then remains stable up to the 20th cycle leading to the polarization of the cell. The broad peak at 0.2 V can be assigned to the alloying reaction.

Secondly, during the first charge, the peak observed at 0.22 V is attributed to the reversible de-alloying reaction and the second oxidation peak at 0.65 V can be assigned to the conversion reaction between Mg^0 and LiH.

Graphite may reversibly store Li in the same voltage range via Li interaction or/and deposition in the available pores (mainly micropores and small mesopores). In our case the contribution of the pristine carbon in the overall capacity of composite was neglected (Figure SI-5). The estimation of the carbon

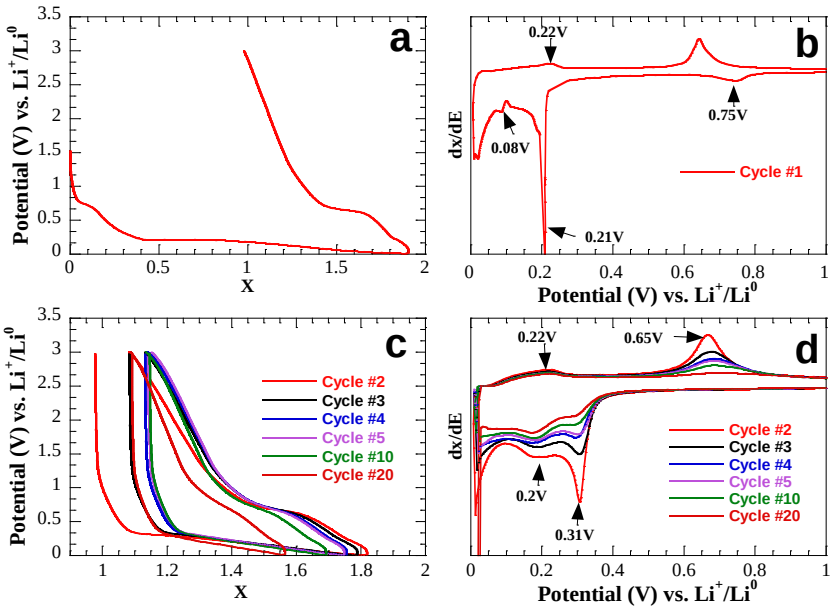

Fig.6 Potential/composition profiles of BM50MgH$_2$@HSAG/Li half cell during the first cycle (a) and from the 2nd to the 20th cycle (c). The corresponding derivative curves (dx/dE) during the first cycle (b) and from the 2nd to the 20th cycle (d).

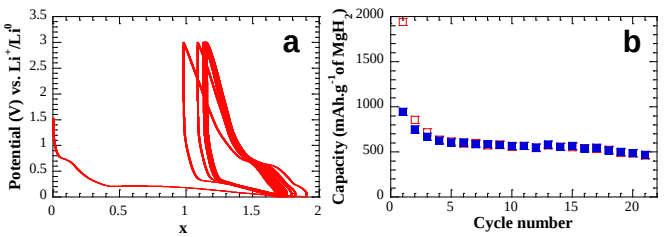

Fig.7 Potential/composition profile of BM50MgH$_2$@HSAG (a); discharge (red) and charge (blue) capacities versus cycle (b).

contribution obtained from the measurements of the pristine carbon (Figure SI-6) is unsuitable. This is mainly due to the nature of the carbon host in the composite, which is strongly modified from the pristine one. In the composite, the carbon pores are filled with the MgH$_2$ nanoparticles and the ball-milling treatment strongly affects both the carbon host crystallinity and porosity, which drastically collapses (Table 1). Therefore, it is very difficult to decouple the contribution of MgH$_2$ from that of the carbon host, which is in any cases very small.

The evolution of the charge and discharge capacities upon cycling is shown in Figure 7. This composite electrode holds a high discharge capacity of 2000 mAh.g^{-1} which fades rapidly to 1000 mAh.g^{-1} for the second discharge. The capacity loss during the first cycle is attributed to the formation of a SEI and to partial irreversibility of the conversion reaction.

Despite the irreversible capacity loss during the first cycle and a slow capacity decrease in the subsequent cycles, the composite electrode shows a remarkable capacity around 500 mAh.g^{-1} after 20 cycles. As compared to the classical top-down preparations of MgH$_2$ that show a rapid capacity drop after few cycles, the present composite offers exceptional cycling life stability.[15,20,21]

The outstanding electrochemical properties in term of cycling life and reversible capacity of the BM50MgH$_2$@HSAG-500 composite is attributed to the bottom-up strategy used for its preparation combined with the ball milling treatment. The synthetic method is able to produce well dispersed MgH$_2$ nanoparticles in the porous carbon host with narrow particles size distribution. The good dispersion of individual nanoparticles and the control of their average size are the main advantages of such bottom-up method as compared to the classical top-down ball milling technique formerly used for metal hydrides. The subsequent ball milling treatment under Ar enhances the electronic contacts between the MgH$_2$ nanoparticles and the carbon host, which leads to a remarkable improvement of electrochemical properties as compared to the as-synthesized composite.

The controlled nanosized of MgH$_2$ particles and the developed porosity of carbon scaffold favour fast reduction/oxidation reactions through large contact areas between MgH$_2$/electrolyte during discharge and better electronic contact at Mg^0/LiH interfaces during charge. Furthermore, nanosizing ensures rapid lithium ions/hydrogen diffusion due to short distances within the nanoparticles.[28]

The developed porous structure of the HSAG-500 carbon allows accommodating the MgH$_2$ volume expansion and subsequently, to hinder the loss of electronic percolation due to repeated volume changes during cycling. Moreover, the presence of carbon scaffold stabilizes the MgH$_2$ nanoparticles upon cycling. After the first discharge and charge cycle, the electrode was characterized by TEM for better understanding of both the stability of particles size and their physical integrity.

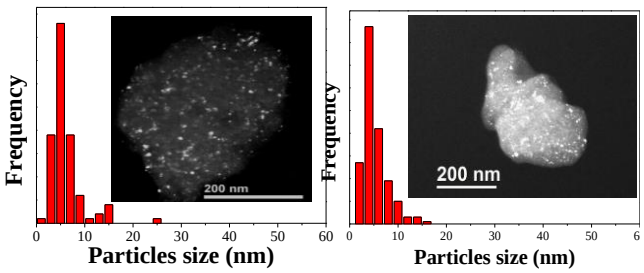

Fig.8 Dark field TEM images and related Mg-based nanoparticles histograms at the end of the first discharge (left) and charge (right) of BM50MgH_2@HSAG-500.

The collected results are depicted in figure 8. TEM dark field images and corresponding histograms show that the particles size distribution of MgH_2 is not affected during the first discharge or charge and the average size range is similar to that before cycling (~ 5.5 nm).

Conclusions

Nanosized MgH_2 particles stabilized into a porous carbon scaffold have been synthesized by a bottom-up method with different metal contents up to 70 wt.% and tested for the first time, to our knowledge, as negative electrode materials for electrochemical conversion reaction with Li.

Tuning the Mg loading allows obtaining controlled MgH_2 nanoparticle size up to a maximum metal concentration of 50 wt.%. For these composites, MgH_2 nanoparticles show narrow particle size distributions and the majority of nanoparticles have sizes below 10 nm with an average size between 4-5.5 nm. The 50 wt.% Mg concentration corresponds to a complete filling of the available carbon porosity with MgH_2 nanoparticles. However, minor porosity still exists for this composite indicating that nanoconfinement of MgH_2 into the pores is partial and MgH_2 nanoparticles are also deposited on the outer surface of the carbon scaffold.

The use of as-prepared powder composites shows poor reversibility of the conversion reaction with Li with a loss of capacity within few cycles suggesting a rapid loss of electronic contact upon cycling.

Strongly improved cycle life stability with a good electrochemical capacity of 500 $mAh.g^{-1}$ is obtained for the same composite after ball milling under Ar. This treatment enhances the electronic contact between the MgH_2 nanoparticles and the carbon host. The nanoparticle size distribution is stable before and after one discharge/charge electrochemical cycle, as determined by TEM analysis.

This result is very encouraging since no electrode formulation has been used to prepare the electrochemical half cells. An appropriate formulation of such composites prepared by bottom-up method will certainly lead to electrodes with advanced electrochemical properties for Li-ion batteries.

Notes and references

[a] *Institut de Chimie et des Matériaux Paris-Est, CNRS UPEC UMR 7182, 2-8 rue Henri Dunant, 94320 Thiais, France*
claudia.zlotea@icmpe.cnrs.fr

[b] *Laboratoire de Réactivité et Chimie des Solides, CNRS UPJV, UMR 7314, 33 rue Saint Leu, 80039 Amiens, France*

†Electronic Supplementary Information (ESI) available: (a) Dark field TEM image and the corresponding SAED electron diffraction pattern of the as-synthesized 15MgH_2@HSAG-500, (b) N_2 sorption isotherms at 77 K of all as-synthesized xMgH_2@HSAG-500 composites, (c) N_2 sorption isotherms at 77 K of 50MgH_2@HSAG-500 composite before and after ball milling, (d) Electrochemical characterizations of all as-synthesized xMgH_2@HSAG-500 composites for the first cycle, where x is 15, 25, 50 and 70 wt.% Mg. (e) Comparison between capacities of two ball milled xMgH_2@HSAG-500 composites with x = 50 and 70 wt.% Mg (f) Electrochemical characterization of the pristine HSAG-500 carbon. See DOI: 10.1039/b000000x/

Funding Sources and acknowledgments

This work was financially supported by the *Université Paris-Est Créteil* (1 year post-doctoral grant) and by the *Foundation d'entreprise EADS – AIRBUS Group* (contract 114-AO12-1209). The authors acknowledge TIMCAL for providing the carbon material, Julie Bourgon for performing TEM measurements and Khaled Bouhlel for precious help with the samples preparation.

1. Q. Zhang, E. Uchaker, S. L. Candelaria, and G. Cao, *Chem. Soc. Rev.*, 2013, **42**, 3127–3171.
2. P. E. de Jongh, M. Allendorf, J. J. Vajo, and C. Zlotea, *MRS Bull.*, 2013, **38**, 488–494.
3. V. Bérubé, G. Radtke, M. Dresselhaus, and G. Chen, *Int. J. Energy Res.*, 2007, 637–663.
4. C. Zlotea and M. Latroche, *Colloids Surf. Physicochem. Eng. Asp.*, 2013, 117–130.
5. F. Schueth, *Chem. Mater.*, 2014, **26**, 423–434.
6. C. Zlotea, C. Chevalier-Cesar, E. Leonel, E. Leroy, F. Cuevas, P. Dibandjo, C. Vix-Guterl, T. Martens, and M. Latroche, *Faraday Discuss.*, 2011, **151**, 117–131.
7. T. K. Nielsen, K. Manickam, M. Hirscher, F. Besenbacher, and T. R. Jensen, *ACS Nano*, 2009, **3**, 3521–3528.
8. Z. Zhao-Karger, J. J. Hu, A. Roth, D. Wang, C. Kubel, W. Lohstroh, and M. Fichtner, *Chem. Commun.*, 2010, **46**, 8353–8355.
9. M. Paskevicius, D. A. Sheppard, and C. E. Buckley, *J. Am. Chem. Soc.*, 2010, **132**, 5077–5083.
10. J. R. Szczech and S. Jin, *Energy Environ. Sci.*, 2011, **4**, 56–72.
11. P. Poizot, S. Laruelle, S. Grugeon, L. Dupont, and J.-M. Tarascon, *Nat. Sept. 28 2000*, 2000, **407**, 496–499.
12. E. García-Tamayo, M. Valvo, U. Lafont, C. Locati, D. Munao, and E. M. Kelder, *J. Power Sources*, 2011, **196**, 6425–6432.
13. X. Shen, S. Chen, D. Mu, B. Wu, and F. Wu, *J. Power Sources*, 2013, **238**, 173–179.
14. M.-Y. Cheng, Y.-S. Ye, T.-M. Chiu, C.-J. Pan, and B.-J. Hwang, *J. Power Sources*, 2014, **253**, 27–34.
15. Y. Oumellal, A. Rougier, G. A. Nazri, J.-M. Tarascon, and L. Aymard, *Nat. Mater.*, 2008, **7**, 916–921.
16. Y. Oumellal, A. Rougier, J.-M. Tarascon, and L. Aymard, *J. Power Sources*, 2009, **192**, 698–702.
17. W. Zaïdi, Y. Oumellal, J.-P. Bonnet, J. Zhang, F. Cuevas, M. Latroche, J.-L. Bobet, and L. Aymard, *J. Power Sources*, 2011, **196**, 2854–2857.
18. Y. Oumellal, W. Zaïdi, J.-P. Bonnet, F. Cuevas, M. Latroche, J. Zhang, J.-L. Bobet, A. Rougier, and L. Aymard, *Int. J. Hydrog. Energy*, 2012, **37**, 7831–7835.
19. Y. Oumellal, M. Courty, A. Rougier, G. A. Nazri, and L. Aymard, *Int. J. Hydrog. Energy*, 2014, **39**, 5852–5857.
20. S. Ikeda, T. Ichikawa, K. Kawahito, K. Hirabayashi, H. Miyaoka, and Y. Kojima, *Chem. Commun.*, 2013, **49**, 7174–7176.
21. S. Brutti, G. Mulas, E. Piciollo, S. Panero, and P. Reale, *J. Mater. Chem.*, 2012, **22**, 14531–14537.
22. M. Konarova, A. Tanksale, J. Norberto Beltramini, and G. Qing Lu, *Nano Energy*, 2012, **2**, 98–104.
23. Y. Liu, J. Zou, X. Zeng, X. Wu, H. Tian, W. Ding, J. Wang, and A. Walter, *Int. J. Hydrog. Energy*, 2013, **38**, 5302–5308.
24. F. Rouquerol, J. Rouquerol, and K. Sing, *Adsorption by Powders and Porous Solids*, Academic Pres., 1999.

25. Y. S. Au, M. K. Obbink, S. Srinivasan, P. C. M. M. Magusin, K. P. de Jong, and P. E. de Jongh, *Adv. Funct. Mater.*, 2014.
26. C. Zlotea, F. Cuevas, J. Andrieux, C. M. Ghimbeu, E. Leroy, E. Léonel, S. Sengmany, C. Vix-Guterl, R. Gadiou, T. Martens, and M. Latroche, *Nano Energy*, 2013, **2**, 12–20.
27. S. Bastide, C. Zlotea, M. Laurent, M. Latroche, and C. Cachet-Vivier, *J. Electroanal. Chem.*, 2013, **706**, 33–39.
28. Y. H. Lee, I. C. Leu, S. T. Chang, C. L. Liao, and K. Z. Fung, *Electrochimica Acta*, 2004, **50**, 553–559.